Adhesion between a rigid cylindrical particle and a soft fluid membrane tube

Jeff Z. Y. Chen and Sergey Mkrtchyan
Department of Physics and Astronomy, University of Waterloo, Waterloo, Ontario, Canada N2L 3G1
(Received 11 January 2010; revised manuscript received 24 February 2010; published 7 April 2010)

We investigate the structure of a tubular membrane adhering to a rigid cylindrical particle, in various radius ratios. Through a theoretical and numerical analysis of a free-energy model that uses Helfrich energy for the description of the membrane, we show that three distinct phases exist, depending on the ratio between radii of the membrane tube and the rigid cylinder and an adsorption parameter describing the attraction between the cylinder and tube surface. The adhesion transition from the desorbed to weakly adhered states is identified as a second-order phase transition; the wrapping transition from the weakly adhered to strongly adhered states is identified as a first-order phase transition.

DOI: 10.1103/PhysRevE.81.041906 PACS number(s): 87.16.D−, 87.15.kt, 68.35.Np

I. INTRODUCTION

Recent theoretical interests in the behavior of macromolecules interacting with fluid membrane surfaces can be attributed to the importance of these systems in both fundamental research and practical soft-matter and biological systems. Profound structural properties have been discovered in the context of simple coarse-grained theoretical models within a few relevant physical parameters, in basic types such as the excluded-volume repulsion and short-ranged surface attraction; these studies have provided understanding of a more complex nature of real soft-matter and biological systems [1–25]. For example, for modeling purposes, a rigid particle of a size competing with a typical length scale in a fluid membrane and attracted to the surface of the membrane by a short-ranged attraction has been used to represent colloids, nanoparticles, or even bacteria. Adhesion (or adsorption) of a single spherical or cylindrical particle to an originally flat membrane was theoretically shown to produce possible stages of phase transitions, ending at a deep engulfing of the membrane sheet about the particle [11,14,18,19,26] when the attraction is significant.

In this paper, we theoretically study the structure of a rigid cylindrical particle of radius R attracted to a freely standing soft cylindrical tube originally of radius r_0, with codirected axes (see Fig. 1). In a cross-section view, this problem is reduced to two dimensions, where we consider the modeling of a rigid circle interacting with a deformable closed curve. The study of this model system serves the purpose of providing a theoretical prediction for the structural properties of systems related to tubular membranes. In addition to a variety of closed shapes normally seen in vesicles, a lipid-bilayer membrane can also be stabilized in a long tubular shape by using a number of experimental techniques [27–32]. Recent experimental and theoretical efforts have been made to examine the structural and transport properties in systems particularly involving tubular membranes [21,23,25,33–38]. The considered system can be simplified into two-dimensional. This can be compared with a number of related systems in two and three dimensions, where progress has been made in understanding the interaction between a vesicle and a flat or curved substrate [1,2,39–42].

To model the fluid membrane we use the Helfrich model that contains two parameters: the bending rigidity κ and surface tension σ [43,44]. Following Seifert and Lipowsky [1], we have further introduced a phenomenological parameter w which describes the adsorption energy per unit area between the contact surfaces of the cylinder and soft tube. In following sections, we show that of the four parameters, κ, σ, w, and R, only two dimensionless combinations are relevant in the consideration of the structure of the current system.

We take the view that the membrane tube is connected to a remote reservoir that maintains a constant tension σ in the system, or equivalently, the considered membrane tube is only a segment of a much longer system where the radius is controlled at a constant value remotely. It is not uncommon in actual experimental setups where the extraction of a tubular membrane requires a much larger vesicle as the "reservoir" [27–32]. We consider that a cylinder of height much shorter than the total length of the membrane tube is ad-

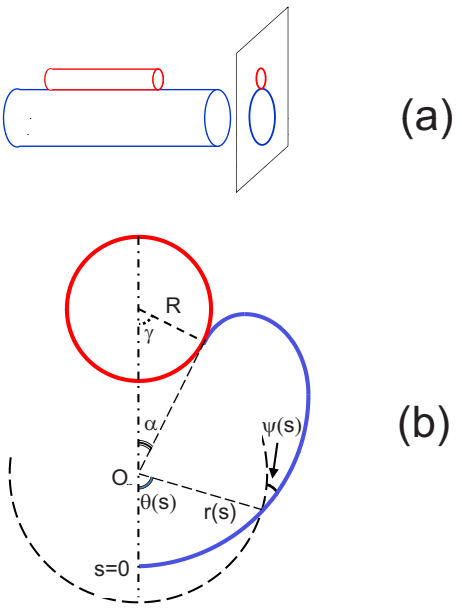

FIG. 1. (Color online) (a) Illustration of the adhesion of a rigid cylindrical particle (red) of radius R to the exterior surface of a soft membrane tube that is originally a right circular cylinder (blue) of radius r_0. The coordinate system used for theoretical calculation is displayed in (b) where the cross-section view perpendicular to the cylinder axis is shown.

sorbed to the surface of the membrane (Fig. 1). Within this section of the system, the area inside and the perimeter about the closed membrane shape curve in Fig. 1(b) are not subject to any constraint. Focusing on this section of the membrane tube alone, we can assume that σ is fixed and the tube has open ends where "membrane material" can be fed or taken away, while the shape undergoes a radial change.

This can be contrasted with a vesicle adhesion problem in three dimensions [1], where the total volume inside the vesicle and the total surface area around the vesicle are normally kept at constant values in a theoretical consideration [45]. In addition to the three-dimensional version, Seifert studied the adhesion problem of vesicles to a flat surface in two dimensions, using a constant "volume" (actually enclosed area in two dimensions) constraint, through a pressure constraint term in the free energy as a two-dimensional version of the three-dimensional problem [2]. To describe an open tubular system connected to a reservoir our current work does not incorporate such a constraint. The inclusion of the constraint in our work is mathematically possible but would describe a different physical setting.

II. FREE-ENERGY MODEL FOR THE FREE PORTION OF THE MEMBRANE

We first define a coordinate system used in this work. We assume the existence of a reflection symmetry of the configuration about a mirror plane, represented by the dash-dot line in Fig. 1(b), which goes through the axis of the rigid cylinder and the original axis of the membrane tube. In a cross section perpendicular to the cylinder axis, only half of the nonadhered portion of the tubular membrane is needed in our calculation. In the sketch, this half portion is represented by a (blue) curve with a path variable s going from $s=0$ to $s=S$.

The shape of the nonadhered portion of the membrane can be specified in terms of polar coordinates $[r(s),\theta(s)]$. At any given s, these two variables can also be related to $\psi(s)$, defined as the angle between the shape line and the coordinate circle of radius $r(s)$ [see Fig. 1(b)], by constraints,

$$\frac{dr}{ds} = \sin\,\psi(s), \tag{1}$$

and

$$r(s)\frac{d\theta}{ds} = \cos\,\psi(s). \tag{2}$$

The use of $\psi(s)$ allows us to write the square bending curvature of the membrane at s as $(d\psi/ds - d\theta/ds)^2$. Taking Eq. (2), we can express the Helfrich free energy for a deformed membrane tube of length L,

$$F = 2L\int_0^S ds\left\{\frac{\kappa}{2}\left[\frac{d\psi}{ds} - \frac{\cos\,\psi(s)}{r(s)}\right]^2 + \sigma\right\}, \tag{3}$$

where L is the length of the rigid cylinder, κ the bending energy and σ surface tension of the membrane surface. In this paper we are interested in a long adhering cylinder $(L/R \gg 1)$ hence ignore the end effects, which amount to a contribution much smaller than the above. A prefactor of 2 has been included to account for two halves of the nonadhering membrane.

We take a moment to examine a trivial solution that can be obtained from the minimization of the free energy in Eq. (3)—the solution of a circle for a free tubular membrane. Letting $\psi(s)=0$ implies $r(s)=r_0=S/\pi$ from Eq. (1) and $\theta(s)=\pi s/S$ from Eq. (2). Inserting these solutions to the free energy in Eq. (3) we obtain

$$\frac{F_0}{2\kappa L} = \frac{\pi^2}{2S} + \frac{\sigma S}{\kappa}. \tag{4}$$

Minimization of Eq. (4) with respect to S yields

$$r_0^2 = (S_0/\pi)^2 = \kappa/(2\sigma), \tag{5}$$

which is the square radius of the tubular membrane, before adhesion of the membrane to the rigid cylinder.

Using r_0 as the basic length scale, we can define dimensionless, reduced length parameters,

$$\tilde{s} \equiv s/r_0, \tag{6}$$

$$\tilde{r} \equiv r/r_0, \tag{7}$$

together with a reduced free energy per unit length,

$$\tilde{F} \equiv \frac{Fr_0}{2\kappa L}. \tag{8}$$

The reduced free energy of the nonadhered portion of the membrane can then be written as

$$\tilde{F}_m = \frac{1}{2}\int_0^{\tilde{S}} d\tilde{s}\left[\left(\frac{d\psi}{d\tilde{s}} - \frac{\cos\,\psi}{\tilde{r}}\right)^2 + 1\right]. \tag{9}$$

Corresponding to the range $\tilde{s}=[0,\tilde{S}]$, the angle $\theta(\tilde{s})$ spans a range $[0,\theta(\tilde{S})]$; within this range of θ, the reduced free energy of the original circular tube of radius r_0, cocentered at the same origin, has the value $\int_0^{\tilde{S}} d\tilde{s}[d\theta/d\tilde{s}]$; taking this free energy as the reference and using the constraint in Eq. (2), we finally arrive at the reduced free-energy difference for the nonadhering portion of the membrane,

$$\Delta\tilde{F}_m = \int_0^{\tilde{S}} d\tilde{s}\left[\frac{1}{2}\left(\frac{d\psi}{d\tilde{s}} - \frac{\cos\,\psi}{\tilde{r}}\right)^2 + \frac{1}{2} - \frac{\cos\,\psi}{\tilde{r}}\right], \tag{10}$$

which needs to be minimized with respect to $\psi(\tilde{s})$ with the constraint,

$$\frac{d\tilde{r}}{d\tilde{s}} = \sin\,\psi(\tilde{s}), \tag{11}$$

a reduced version of Eq. (1).

The functional minimization problem can be treated in comparison with the formalism developed in classical mechanics. We introduce an effective Lagrangian

$$L = \frac{1}{2}\left(\dot{\psi} - \frac{\cos\psi}{\tilde{r}}\right)^2 + \frac{1}{2} - \frac{\cos\psi}{\tilde{r}} + \lambda(\tilde{s})[\dot{\tilde{r}} - \sin\psi(\tilde{s})], \tag{12}$$

where $\lambda(\tilde{s})$ is a Lagrangian multiplier function to be determined below, and a dotted symbol represents a derivative with respect to $\tilde{s}$. Effective canonical momenta can then be introduced,

$$P_\psi(\tilde{s}) \equiv \frac{\partial L}{\partial \dot{\psi}} = \dot{\psi} - \frac{\cos\psi}{\tilde{r}}, \tag{13}$$

and

$$P_r(\tilde{s}) \equiv \frac{\partial L}{\partial \dot{\tilde{r}}} = \lambda(\tilde{s}). \tag{14}$$

It turns out that in the current problem $P_\psi(\tilde{s})$ has the simple physical meaning of the membrane curvature at $\tilde{s}$. Using the effective Lagrangian, we can define an effective Hamiltonian,

$$H = P_\psi\dot{\psi} + P_r\dot{\tilde{r}} - L = \frac{P_\psi^2}{2} + \frac{P_\psi\cos\psi}{\tilde{r}} + \frac{\cos\psi}{\tilde{r}} - \frac{1}{2} + P_r\sin\psi. \tag{15}$$

The use of Hamilton's equations of motion then leads to four first-order differential equations to be solved for four functions $\tilde{r}(\tilde{s})$, $\psi(\tilde{s})$, $P_r(\tilde{s})$, and $P_\psi(\tilde{s})$,

$$\frac{d\psi}{d\tilde{s}} = P_\psi + \frac{\cos\psi}{\tilde{r}}, \tag{16}$$

$$\frac{d\tilde{r}}{d\tilde{s}} = \sin\psi, \tag{17}$$

$$\frac{dP_\psi}{d\tilde{s}} = (P_\psi + 1)\frac{\sin\psi}{\tilde{r}} - P_r\cos\psi, \tag{18}$$

and

$$\frac{dP_r}{d\tilde{s}} = \frac{(P_\psi + 1)\cos\psi}{\tilde{r}^2}. \tag{19}$$

Four initial conditions are needed to completely specify the conditions required for solving the above equation set. We use

$$\psi(0) = 0, \tag{20}$$

which is a condition that the shape curve at $\tilde{s}=0$ has a zero slope because of the mirror symmetry, and

$$\tilde{r}(0) = 1, \tag{21}$$

which removes the ambiguity in selecting the origin of the coordinate system along the dash-dotted line in Fig. 1(b). We also use two varying parameters, ξ and ζ,

$$P_\psi(0) = \xi \quad \text{and} \quad P_r(0) = \zeta, \tag{22}$$

in our calculation. Once ξ, ζ, and $\tilde{S}$ are given, the solution to the differential equations gives trajectories of the four functions from $\tilde{s}=0$ to $\tilde{s}=\tilde{S}$.

Within this treatment, mathematically the function $\theta(\tilde{s})$ is not directly involved. The integration to find $\theta(\tilde{s})$ is straightforward and can be conducted after the trajectories have been calculated, from,

$$\theta(\tilde{s}) = \int_0^{\tilde{s}} dt\,\cos\psi(t)/\tilde{r}(t). \tag{23}$$

At $\tilde{s}=\tilde{S}$, the membrane curve tangentially connects to the other portion which is adhered to the surface of the rigid cylinder. In the next section, we are interested in discussing the physical properties of the adhesion problem with attention paid to an adhering cylinder of radius R and wrapping angle γ [see definitions in Fig. 1(b)] as basic physical parameters. This further produces two connection conditions at $\tilde{S}$; one of which is

$$\gamma = \theta(\tilde{S}) - \psi(\tilde{S}) - \pi, \tag{24}$$

and the other is

$$R/r_0 \equiv \tilde{R} = \frac{\tilde{r}(\tilde{S})\sin[\theta(\tilde{S})]}{\sin\gamma}. \tag{25}$$

At this stage, on the basis of how these quantities are calculated, we can take the mathematical perspective that by using ξ, ζ and $\tilde{S}$ as the initial parameters, the functions

$$\tilde{R} = \tilde{R}(\xi, \zeta; \tilde{S}) \tag{26}$$

and

$$\gamma = \gamma(\xi, \zeta; \tilde{S}), \tag{27}$$

can be calculated together with

$$\Delta\tilde{F}_m = \Delta\tilde{F}_m(\xi, \zeta; \tilde{S}) \tag{28}$$

yielded from Eq. (10), after a solution to the differential Eqs. (16)–(19) is found with initial conditions (20)–(22).

Considering the more interesting $\tilde{R}$ and γ as physical parameters of the system, we can also take another perspective, namely, regarding both ξ and ζ as functions of $\tilde{R}$ and γ as well as $\tilde{S}$. In this view, the above free-energy difference becomes a function of $\tilde{R}$, γ and $\tilde{S}$. For fixed $\tilde{R}$ and γ, varying $\tilde{S}$ we can search for the location of the free-energy minimum, $\tilde{S}_0$. This free-energy minimum,

$$f_m(\tilde{R}, \gamma) \equiv \Delta\tilde{F}_m[\xi(\tilde{R}, \gamma, \tilde{S}_0), \zeta(\tilde{R}, \gamma, \tilde{S}_0); \tilde{S}_0], \tag{29}$$

is then used in Sec. III for analysis of the physical problem. The numerical procedure designed to handle the transformation from Eqs. (26)–(28) to Eq. (29) is discussed in Appendix A; readers who are not interested in numerical techniques can proceed directly to Sec. III.

III. RESULTS AND DISCUSSION

In this section, we assume that a short-range potential energy per unit area, w (negative), can be attained when the membrane and cylinder surfaces are in contact. The same parameter was introduced in related systems recently [1,2,14,18,19,25,26]. Taking into account the bending and tension energies, we can write the reduced free-energy difference for the contact portion of the system,

$$\Delta\tilde{F}_{\text{contact}} = \tilde{w}\gamma\tilde{R} + \frac{1}{2}\left(\frac{1}{\tilde{R}^2} + 1\right)\gamma\tilde{R} - \alpha, \tag{30}$$

where the last term is the reduced reference free energy of a tubular membrane corresponding to the angle α specified in Fig. 1(b). In Eq. (30), we have also introduced a reduced adhesion energy,

$$\tilde{w} = wr_0^2/\kappa, \tag{31}$$

important in the following discussion.

Adding the contribution from the nonadhered portion of the membrane discussed in the last section to Eq. (30), we arrive at the total reduced free-energy difference of the system,

$$\Delta\tilde{F}(\tilde{R},\gamma,\tilde{w}) = f_m(\tilde{R},\gamma) + \tilde{w}\gamma\tilde{R} + \frac{1}{2}\left(\frac{1}{\tilde{R}^2} + 1\right)\gamma\tilde{R} - \alpha, \tag{32}$$

where $f_m(\tilde{R},\gamma)$ is the contour-minimized free-energy difference in Eq. (29). From the relationship in Eq. (24), we have

$$\alpha = -\gamma - \psi(\tilde{R},\gamma), \tag{33}$$

where $\psi(\tilde{R},\gamma)$ is the angle ψ at the contact point $\tilde{S}$, which, after the minimization with respect to all possible paths that the free portion of the membrane can make, as discussed in the last section, is a function of $\tilde{R}$ and γ. In the geometry shown in Fig. 1(b), the terminal ψ has a negative value hence α can be shown to be positive.

A. Second-order adhesion transition from desorption to weak wrapping

For fixed $\tilde{R}$, increasing the reduced adhesion energy $|\tilde{w}|$ induces an adhesion transition between a desorption state, where the rigid cylinder and the membrane have no contact, to a weak-wrapping state, where the configuration resembles Fig. 1(a) with a small wrapping angle γ and weak membrane shape distortion. In this section, we show that this phase transition can be determined analytically without invoking the numerical analysis in Appendix A. The characteristic property of this transition is the wrapping angle γ.

In Appendix B, we show that in weak adhesion, to linear order in $\psi(\tilde{S})$ the contribution of $f_m(\tilde{R},\gamma)$ to the total energy is simply $-\psi(\tilde{S})$. The use of this term and the expression of α, Eq. (33), in Eq. (32) gives

$$\Delta\tilde{F}(\tilde{R},\gamma,\tilde{w}) = \left[\left(\frac{1}{2\tilde{R}^2} + \frac{1}{2} + \tilde{w}\right)\tilde{R} + 1\right]\gamma + \mathcal{O}(\gamma^2). \tag{34}$$

Although the coefficient of the γ^2 term is not explicitly calculated in this work, it must be positive; otherwise, if the coefficient was negative, the system would undergo a spontaneous shape distortion even *without* the presence of attraction to the rigid cylinder. Indeed, in Eq. (4) of Ref. [18] and Eq. (15) of Ref. [26], we see similar free-energy expansions of related systems, where the coefficient of the quadratic wrapping-angle term is positive.

This expansion allows us to identify an "order parameter" $\sqrt{\gamma}$, in comparison with the standard Ginzburg-Landau free-energy expansion of a second-order phase transition. As $\tilde{w}$ is small, the free energy has a minimum at $\gamma_0=0$, representing no contact between the membrane and the cylinder, hence the system is in a desorption state. Beyond a critical $\tilde{w}_c$, the first term in Eq. (34) becomes negative at a nonzero, small γ_0, indicating an adhesion between membrane and the rigid cylinder surface. The critical point is determined by the requirement that the coefficient of the γ term vanishes, which can be solved to yield

$$\tilde{w}_c = -\frac{1}{2}\left(1 + \frac{1}{\tilde{R}}\right)^2. \tag{35}$$

In the phase diagram presented in Fig. 2, the curve associated with overlaying squares represents this analytic result for the phase boundary.

An interesting limit of the critical adhesion energy in Eq. (35) can be considered by taking $R \ll r_0$,

$$w_c = -\frac{\kappa}{2R^2}, \tag{36}$$

which coincides with the critical adhesion energy for the system of a rigid cylinder adhering to a flat membrane studied in Ref. [26]. A simple interpretation of this w_c is that as the adhesion transition takes place, the bending energy penalty per unit area occurring in the membrane is compensated by the adhesion-energy gain per unit area.

Another interesting limit of the critical adhesion energy in Eq. (35) is for the case of adhesion between a soft tubular membrane of radius r_0 and a flat, rigid surface, when $R \gg r_0$,

$$w_c = -\frac{\kappa}{2r_0^2}. \tag{37}$$

This can be understood from a balance of energetics in the system as well; the entire adsorbed area of the membrane to the flat surface is flat hence the free-energy loss per unit area, in reference to that of a tubular membrane of radius r_0, is $\kappa/2r_0^2$. An adhesion transition takes place as the adhesion-energy gain compensates this loss. The above critical adsorption, Eq. (37), agrees with that determined in [2]. At the onset of the transition, the membrane shape remains almost a perfect circle where the area inside is not changed; the systems considered here and in [2] hence have the same characteristics.

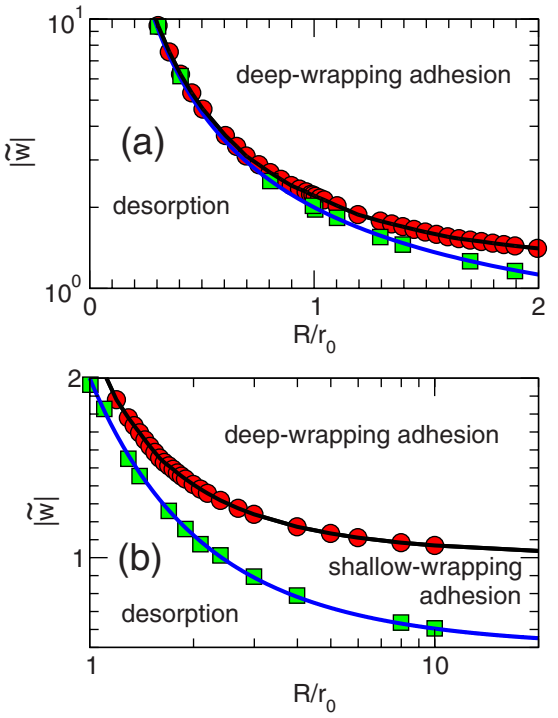

FIG. 2. (Color online) Phase diagram for the adhesion of a cylinder of radius R to an originally cylindrical membrane of radius r_0, in a parameter space spanned by the reduced adhesion energy $|w|r_0^2/\kappa$ and radius ratio R/r_0. Two separate plots, (a) and (b), are shown for different regions of the phase diagram. The curve associated with square symbols is a second-order phase boundary between the desorbed and weak-adhesion states where the tubular membrane shows a weak shape distortion, determined from a Ginzburg-Landau free-energy expansion. Circles represent our numerical results for the first-order phase boundary between the weak-adhesion and strong-adhesion states where the membrane deeply wraps the rigid cylinder.

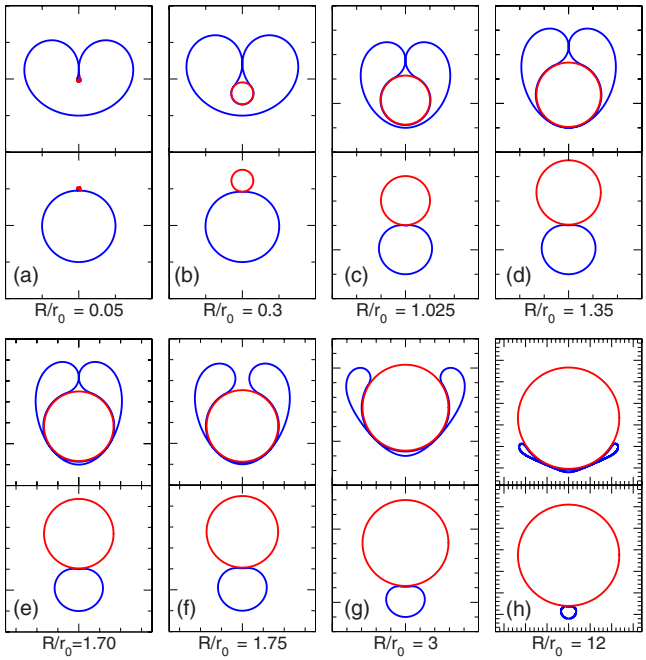

FIG. 3. (Color online) Cross-section profiles of the tubular membrane (blue) at the first-order phase transition from deep wrapping (upper panels) to shallow wrapping (lower panels) around the rigid cylinder (red). The shapes were plotted according to numerical results obtained in this work for various radius ratios R/r_0, where R is the radius of the rigid cylinder and $r_0=\sqrt{\kappa/(2\sigma)}$ the radius of the soft membrane tube before adhesion takes place.

Although we have derived the second-order transition boundary analytically using a small-angle expansion, we can also determine this phase transition independently on the basis of analyzing numerical results described in Appendix A. The function $f_m(\tilde{R},\gamma)$ can be computed numerically and listed in a lookup table. For every set of fixed $\tilde{R}$ and $\tilde{w}$, we numerically search for the minimum of $\Delta\tilde{F}(\tilde{R},\gamma,\tilde{w})$ as a function of γ. At small values of $\tilde{w}$, the only free-energy minimum has a value of zero and corresponds to $\gamma_0=0$; the system is in a desorption state. The set $\tilde{R}$ and $\tilde{w}_c$ represents a critical point, once the searched minimum of $\Delta\tilde{F}(\tilde{R},\gamma_0,\tilde{w})$ becomes weakly negative. In this way, critical points can be determined numerically and are represented in Fig. 2 by (green) squares. The agreement with the analytic result is excellent.

B. First-order wrapping transition from weak to deep wrapping

At a fixed $\tilde{R}$, beyond a second-order adhesion transition $\tilde{w}_c$, more distortion of the membrane cross section can be seen but the entire conformation remains approximately circular. Characteristically, the weakness of the distortion is reflected in the smallness of the wrapping angle γ_0 (corresponding to the free-energy minimum), typically much smaller than $\pi/2$. As $|\tilde{w}|$ reaches another transition point, $\tilde{w}_w$, a first-order transition from the weak-wrapping state to the deep-wrapping state takes place. In the deep-wrapping conformation, a major portion of the cylinder is in contact with the membrane. There is no analytic solution for determination of this phase boundary. The phase boundary was numerically determined and is represented in Fig. 2 by circles, where a solid line has also been drawn over the circles as guidance for eyes. For a number of different radius ratios R/r_0, in Fig. 3 we illustrate the conformation of the system at the transition boundary.

The numerical procedure used to determine this phase transition relies on the analysis of the lookup table for the function $f_m(\tilde{R},\gamma)$. Using this table we search for the minimum of $\Delta\tilde{F}(\tilde{R},\gamma,\tilde{w})$ as a function of γ for given values of $\tilde{R}$ by gradually increasing $|\tilde{w}|$. Near the wrapping transition $\tilde{w}_w$, two minima are typically seen: one corresponding to a shallow-wrapping state and the other deep-wrapping. At the transition $\tilde{w}_w$, the two minima have an equal value. A typical $\Delta\tilde{F}(\tilde{R},\gamma,\tilde{w}_w)$ for $\tilde{R}=4$ as a function of γ is shown in Fig. 4(a), where a free-energy barrier having a barrier height δ can be seen between two free-energy minima having a well depth ϵ. For various values of $\tilde{R}$, in Fig. 4(b) δ and ϵ are shown in reduced units by open and filled circles, respectively. As an indication of the magnitude, according to Eqs.

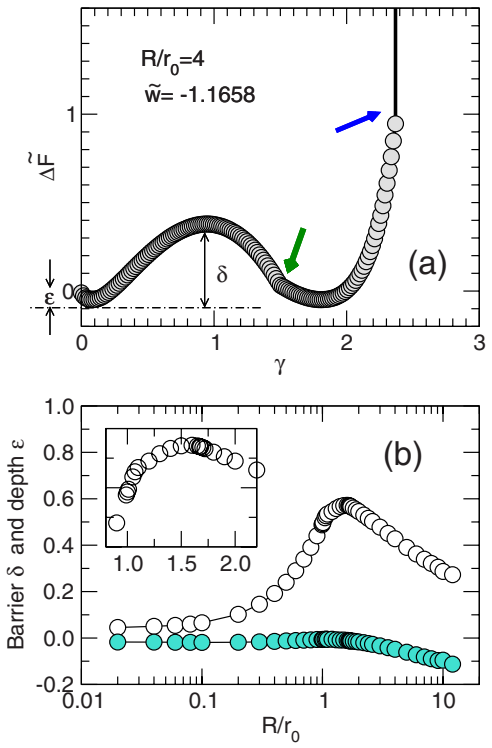

FIG. 4. (Color online) Characteristics of the reduced free-energy difference at the first-order transition. Shown in plot (a) is the reduced free-energy difference [Eq. (34)] as a function of the wrapping angle γ at the first-order transition between shallow and deep wrappings for $R/r_0=4$. The well depth ϵ and barrier height δ are defined and two arrows specify other features discussed in the text. Filled and open symbols in (b) represent ϵ and δ for the range of R/r_0 considered in this work.

(4)–(8), a free membrane tube has a reduced free energy per unit length in the magnitude of $F_0 r_0/(2\kappa L)=\pi$.

A careful examination of free-energy curves for various values of $\tilde{R}$ reveals a number of interesting properties of the deep-wrapping state, after the wrapping transition. Typical conformations of the system for $\tilde{R}=0$ to $\tilde{R}\approx 1.1$ are illustrated in the first three plots of Fig. 3, where the wrapping membrane touches itself from the left to right sides on the top of the wrapped cylinder. The free-energy plots as functions of γ have slightly different features from the example given in Fig. 4(a); the sharp bending of the curve indicated by the down-pointing arrow, for example, does *not* exist. The free-energy curve first displays a minimum at a small γ where a shallow-wrapping state is stabilized, ascents to reach a free-energy barrier and then descents to a second free-energy minimum. Within this range of $\tilde{R}$, the location of the second minimum, where the deep-wrapping state resides at the wrapping transition, is determined by the limit in γ at which the two wings of the membrane start to touch each other on the top of the wrapped cylinder. This limit, at a rather large value of γ, is noted in Fig. 4(a) by a upper-pointing arrow, interrupts the smooth variation in the free-energy curve. The adsorption height, defined as the distance from the bottom of the cylinder to the bottom of the membrane curve, H, the wrapping angle γ_0, and the membrane

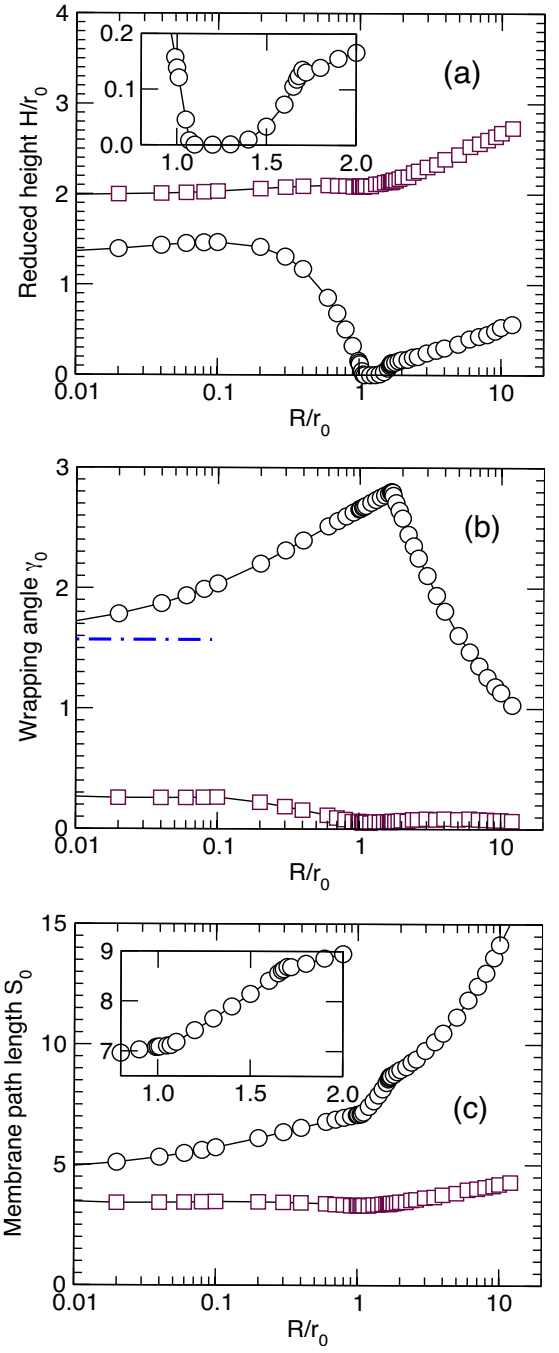

FIG. 5. (Color online) Distance from the bottom of the adhered cylinder to the bottom of the adhering membrane H, wrapping angle γ_0, and half membrane size S_0, as functions of the radius ratio R/r_0 for deep-wrapping and shallow-wrapping states (circles and squares, respectively) at the wrapping transition $\tilde{w}_w$. In plot (b), we have also indicated the limit of the wrapping angle $\gamma_0=\pi/2$ for the deep-wrapping state by a dash-dotted line, valid for $R/r_0\to 0$.

path length of the nonadhered portion S_0, are shown by circles in Fig. 5 and can be seen to vary smoothly in the specified region of $\tilde{R}$. For comparison, these physical properties for the coexisting shallow-wrapping conformations at the first-order wrapping transition $\tilde{w}_w$, are shown in Fig. 5 by squares. Approximately at $\tilde{R}\approx 1.1$, the adsorption height H

reaches zero as the bottom of the membrane portion adhered to the cylinder touches the bottom of the nonadhered membrane.

The deep-wrapping conformation for $\tilde{R}$ in the range of $\tilde{R} \approx 1.1$ to $\tilde{R} \approx 1.7$ has somewhat different characteristics. The calculation of the shape of the nonadhered membrane portion was performed under yet another additional constraint so that the shape curve does not cut into the red circle in Fig. 3, i.e., this portion of the membrane is required to be excluded from the interior of the rigid cylinder. The direct result of invoking this constraint is the occurrence of a cusp in the free-energy curve, indicated in Fig. 4(a) by a down-pointing arrow, dividing the region into two: smaller γ where the shape curve is not subject to this additional constraint and larger γ subject to the constraint. As a consequence, from $\tilde{R} \approx 1.1$ to $\tilde{R} \approx 1.7$, the adsorption height H characteristically rises from zero to a finite value again, first slowly and then more drastically; a signature of this range can also be detected in the S_0 curve as a function of $\tilde{R}$; these can be viewed in the insets of Fig. 5.

For systems in the range of $\tilde{R} \approx 1.7$ to 12, the free-energy curve is characteristically very similar to the plot in Fig. 4(a), where the second minimum (corresponding to the deep-wrapping conformation at the wrapping transition) shows up before the limit where two wings of the wrapping membrane touch each other. The last three illustrations in Fig. 3 represent this type of conformations. In particular, one can see that the wrapping angle γ_0 of the deep-wrapping state starts to retreat from a maximal value [Fig. 5(b)] in this range of $\tilde{R}$. The two wrapping wings on the top of the rigid cylinder are now no longer in contact.

C. Contact curvature in the weak-wrapping state

In this work, we assume that the membrane shape curve connects with the cylinder surface tangentially through a zero contact angle. It is interesting to examine the (nonzero) curvature at the contact point (the "contact curvature") and relate that with other parameters in the system. Seifert [2] showed that the difference between the curvature of the membrane at the contact point, $r_0 P_\psi(\tilde{S})$ in our notation, and the curvature of the substrate, $1/R$ in our notation, is related to the adhesion-energy $\tilde{w}$, through a simple relationship,

$$[P_\psi(\tilde{S}) - 1/\tilde{R}]^2(\text{contact point}) = 2|\tilde{w}|, \tag{38}$$

where we have written all quantities in reduced units. Note that the right-hand side does not depend on $\tilde{R}$ hence the relationship is common for all $\tilde{R}$, because of the local nature of the contact point.

This is a remarkable relation which can be tested by our numerical results. In Fig. 6 we plot the left-hand side of the above expression, calculated by using numerical data of $P_\psi(\tilde{S})$ from the minimization problem in this work, as a function of $\tilde{w}$ in the range where the weak-wrapping state is stable, for various values of $\tilde{R}$. As we can see from the figure, our numerical solution completely agrees with the expected theoretical result in Eq. (38), shown by a straight line. For any given $\tilde{R}$, there is a limited region in $\tilde{w}$ where the weak-wrapping state is stable; this region can be visually small in a logarithmic scale, reflected in the figure by densely overlapping symbols.

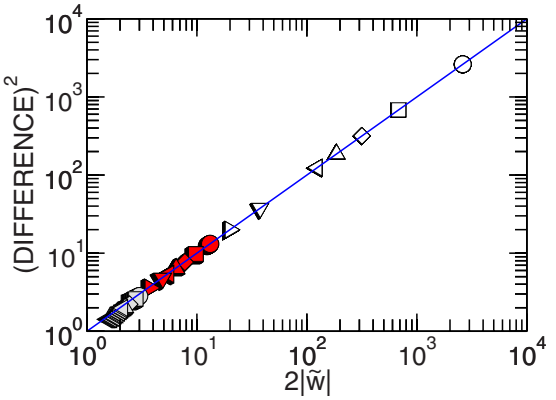

FIG. 6. (Color online) Numerical results for the square of the difference between the curvature of free membrane portion and the curvature of the wrapped cylinder at the contact point $s=S$ as a function of $\tilde{w}$, for various values of $\tilde{R}$. Presented in open symbols, circles, squares, diamonds, up triangles, left triangles, down triangles and right triangles correspond to $\tilde{R}=0.02$, 0.04, 0.06, 0.08, 0.1, 0.2, and 0.3, respectively. Presented in symbols filled with red color, circles, squares, diamonds, up triangles, left triangles, down triangles, and right triangles correspond to $\tilde{R}=0.4$, 0.5, 0.6, 0.7, 0.8, 0.9, and 1.2, respectively. Presented in symbols filled with light gray color, circles, squares, diamonds, up triangles, and left triangles correspond to $\tilde{R}=1.7$, 2, 3, 5, and 10, respectively. Overlaying is a straight line representing the theoretical result, Eq. (38), from Ref. [2].

Note that Eq. (38) is the result of minimization of the system energy Eq. (32) with respect to γ, *not* a boundary condition for the contact curvature to start with [2]. Within similar mathematical steps to those in the Appendix of Ref. [18] we can analytically show that Eq. (38) is the result of minimizing the free energy in Eq. (32). In this paper, we do not repeat this analytical derivation, rather demonstrate the concept by using numerical data in Fig. 6.

IV. SUMMARY

We have investigated phases that can form when a long rigid cylinder of radius R interacts with a membrane tube of radius r_0, where the axes of the two are in parallel, through an excluded-volume interaction and a short-ranged attraction represented by a potential energy per unit area w. We have used the Helfrich energy to characterize the free energy of the membrane, which possesses a bending energy κ. As shown in Secs. II and III, of the three parameters, only two combinations, R/r_0 and wr_0^2/κ, are relevant in the model.

We have developed a numerical procedure that allows us to calculate the free energy of the system in a large range of R/r_0. The analysis of the free energy leads to the conclusion that two phase transitions exist in this simple system. In an adhesion transition, the rigid cylinder makes a contact with

the membrane tube where the cross-section shape remains almost circular; both analytical and numerical analyses support that the adhesion transition is second order. In a wrapping transition at a larger wr_0^2/κ, the membrane shape makes an abrupt change from shallow wrapping to deep wrapping about the cylinder; our numerical analysis of the free energy and a number of other physical properties identifies this as a first-order phase transition.

The physical properties of free-energy curves and conformations of deep-wrapping states show different characteristics in three ranges of R/r_0 identified in Sec. III at the first-order wrapping transition. We used the wrapping angle γ_0, the reduced adsorption height H/r_0, and the reduced membrane size of the nonadhered portion S_0/r_0 to further describe the conformational behavior in these three ranges of R/r_0.

The radius of the membrane tube, r_0, is related to the surface tension of the tubular membrane σ by $r_0^2=\kappa/2\sigma$. In view of the fact that r_0 can be adjusted through the tension σ, a possible experimental test of the phase transitions predicted from this study can be done by varying σ. For fixed R and w, this corresponds to a special trajectory in the phase diagram described in Sec. III where R/r_0 and wr_0^2/κ are used as parameters.

It would be interesting to include a constant enclosed area constraint in our model, which can be used to describe a two-dimensional version of a spherical particle interacting with a vesicle. Pushing to the limit $\tilde{R}\gg 1$, such a study would recover the problem of adhesion of a two-dimensional vesicle to a flat substrate, previously studied by Seifert [2].

ACKNOWLEDGMENTS

We thank the Natural Science and Engineering Research Council of Canada for financial support and SHARCNET for providing computational time.

APPENDIX A: NUMERICAL APPROACH IN MEMBRANE SHAPE CALCULATION

Most analysis in this paper depends on the integration of Eqs. (16)–(19), which can be performed by using the Runge-Kutta algorithm. The integration step length was taken to be

$$\delta\tilde{S}=0.0001 \tag{A1}$$

in integrating the numerical system.

There are three parameters in the integration system, ξ, ζ and $\tilde{S}$. Two of them are related to $\tilde{R}$ and γ by constraints in Eqs. (26) and (27). For each integration range $\tilde{S}$, we used a shooting method to numerically solve Eqs. (16)–(19) using $\tilde{R}$ and γ as a target. That is, an algorithm was designed to vary both ξ and ζ such that the solution to Eqs. (16)–(19) will match prespecified values of $\tilde{R}$ and γ according to Eqs. (26) and (27) at $\tilde{s}=\tilde{S}$. This method has proven to be useful and was implemented in the calculation of the membrane shape [18]. In this work we found that Newton's method for root finding of two-variable equations is convenient for carrying out the shooting procedure. Note that not all $\tilde{S}$ yield valid prespecified shooting target $\tilde{R}$ and γ. Also implemented in this part of the numerical procedure are two additional constraints so that (I) in deep wrapping the two wings of the membrane do not overlap with each other on top of the wrapped cylinder (see Fig. 3) and (II) the shape curve never cuts into the circular shape representing the rigid cylinder.

The reduced free-energy difference $\Delta\tilde{F}_m$, Eq. (28), can then be regarded as a function of $\tilde{R}$, γ, and $\tilde{S}$, determined by the above numerical procedure. The minimization of $\Delta\tilde{F}_m$ with respect to $\tilde{S}$ is then considered. Depending on values of $\tilde{R}$ and γ, in most parameter region, the minimization can be effectively carried out by numerically solving $d[\Delta\tilde{F}_m]/d\tilde{S}=0$ to yield the location $\tilde{S}_0$ for the free-energy minimum. However, in some parameter regions, the imposition of constraints (I) and (II) spoils the continuity of $d[\Delta\tilde{F}_m]/d\tilde{S}=0$ in such a way that a numerical derivative cannot be reliably produced; in this case, the free-energy minimum was found by directly searching the $\tilde{S}$ space.

Implementing these numerical procedures, we can calculate the function $f_m(\tilde{R},\gamma)$ in Eq. (29), which is represented in a look-up table with values of $\tilde{R}$ shown in Fig. 4(b) and γ varying in a small increment,

$$\delta\gamma=0.00005. \tag{A2}$$

This table also contains all other physical properties needed for the solution of the problem and is used for data analysis in Sec. III. The numerical errors yielded from this calculation are smaller than the size of symbols we used to plot the results in figures.

As a final note, our computational implementation of the shooting method becomes unstable for $\tilde{R}\geq 12$ in the deep-wrapping region, even in double precisions; the target becomes too sensitive to the initial selection of ξ and ζ. We have not yet found another stable numerical method to perform the calculation of the phase diagram going beyond $\tilde{R}\geq 12$.

APPENDIX B: SMALL WRAPPING-ANGLE EXPANSION OF THE FREE-ENERGY DIFFERENCE IN (9)

In Sec. III A, we used a small wrapping-angle expansion of the free energy in Eq. (9), when the cross section of the free portion of the membrane undergoes a small distortion from a perfect circular shape. The derivation is considered in more details here. For the free portion of the membrane, we rewrite Eq. (9) as

$$\Delta\tilde{F}_m=\int_0^{\tilde{S}}d\tilde{s}\left[\frac{1}{2}\left(\frac{d\psi}{d\tilde{s}}\right)^2-\frac{d\psi}{d\tilde{s}}\frac{\cos\psi}{\tilde{r}}+\frac{1}{2}\left(\frac{\cos\psi}{\tilde{r}}-1\right)^2\right]. \tag{B1}$$

Corresponding to a circular shape, the zeroth order of a weakly deformed membrane shape, $\psi_0=0$ and $\tilde{r}_0=1$. To the zeroth order, $\Delta\tilde{F}_m\simeq 0$. When the membrane profile makes weak distortions, keeping a term of linear order in ψ and dropping all higher-order terms, we have

$$\Delta\tilde{F}_m \approx \int_0^{\tilde{S}} d\tilde{s}\left(-\frac{d\psi}{d\tilde{s}}\right) = \psi(0) - \psi(\tilde{S}) = -\psi(\tilde{S}), \quad \text{(B2)}$$

where we used the initial condition (20) in the last step.

[1] U. Seifert and R. Lipowsky, Phys. Rev. A **42**, 4768 (1990).
[2] U. Seifert, Phys. Rev. A **43**, 6803 (1991).
[3] C. Hiergeist, V. A. Indrani, and R. Lipowsky, Europhys. Lett. **36**, 491 (1996).
[4] K. Yaman, P. Pincus, and C. M. Marques, Phys. Rev. Lett. **78**, 4514 (1997).
[5] R. Lipowsky and H.-G. Dobereiner, Europhys. Lett. **43**, 219 (1998).
[6] Y. W. Kim and W. Sung, Europhys. Lett. **47**, 292 (1999).
[7] M. Breidenich, R. R. Netz, and R. Lipowsky, Europhys. Lett. **49**, 431 (2000).
[8] M. Breidenich, R. R. Netz, and R. Lipowsky, Eur. Phys. J. E **5**, 403 (2001).
[9] Y. W. Kim and W. Sung, Phys. Rev. E **63**, 041910 (2001).
[10] I. Tsafrir, D. Sagi, T. Arzi, M.-A. Guedeau-Boudeville, V. Frette, D. Kandel, and J. Stavans, Phys. Rev. Lett. **86**, 1138 (2001).
[11] A. Boulbitch, Europhys. Lett. **59**, 910 (2002).
[12] M. Laradji, Europhys. Lett. **60**, 594 (2002).
[13] T. Bickel, J. Chem. Phys. **118**, 8960 (2003).
[14] T. R. Weikl, Eur. Phys. J. E **12**, 265 (2003).
[15] A.-S. Smith, E. Sackmann, and U. Seifert, Europhys. Lett. **64**, 281 (2003).
[16] M. Laradji, J. Chem. Phys. **121**, 1591 (2004).
[17] A.-S. Smith, E. Sackmann, and U. Seifert, Phys. Rev. Lett. **92**, 208101 (2004).
[18] M. Deserno, Phys. Rev. E **69**, 031903 (2004).
[19] M. Deserno, J. Phys.: Condens. Matter **16**, S2061 (2004).
[20] T. Auth and G. Gompper, Phys. Rev. E **72**, 031904 (2005).
[21] F. Brochard-Wyart, T. Tanaka, N. Borghi, and P.-G. de Gennes, Langmuir **21**, 4144 (2005).
[22] M. M. Muller, M. Deserno, and J. Guven, Phys. Rev. E **76**, 011921 (2007).
[23] J. Z. Y. Chen, Phys. Rev. Lett. **98**, 088302 (2007).
[24] B. Rozycki, R. Lipowsky, and T. R. Weikl, Europhys. Lett. **84**, 26004 (2008).
[25] J. Z. Y. Chen, Y. Liu, and H. J. Liang, Phys. Rev. Lett. **102**, 168103 (2009).
[26] S. Mkrtchyan, C. Ing, and J. Z. Y. Chen, Phys. Rev. E **81**, 011904 (2010).
[27] J. Dai and M. P. Sheetz, Biophys. J. **77**, 3363 (1999).
[28] N. Borghi, O. Rossier, and F. Brochard-Wyart, Europhys. Lett. **64**, 837 (2003).
[29] A. Karlsson, R. Karlsson, M. Karlsson, A.-F. Cans, A. Stromberg, F. Ryttsen, and O. Orwar, Nature (London) **409**, 150 (2001).
[30] A. Roux, G. Cappello, J. Cartaud, J. Prost, B. Goud, and P. Bassereau, Proc. Natl. Acad. Sci. U.S.A. **99**, 5394 (2002).
[31] I. Tsafrir, Y. Caspi, M. A. Guedeau-Boudeville, T. Arzi, and J. Stavans, Phys. Rev. Lett. **91**, 138102 (2003).
[32] O. Campas, C. Leduc, P. Bassereau, J. Casademunt, J.-F. Joanny, and J. Prost, Biophys. J. **94**, 5009 (2008).
[33] I. Derenyi, F. Julicher, and J. Prost, Phys. Rev. Lett. **88**, 238101 (2002).
[34] T. R. Powers, G. Huber, and R. E. Goldstein, Phys. Rev. E **65**, 041901 (2002).
[35] M. Tokarz, B. Akerman, J. Olofsson, J.-F. Joanny, P. Dommersnes, and O. Orwar, Proc. Natl. Acad. Sci. U.S.A. **102**, 9127 (2005).
[36] M. Tokarz, B. Hakonen, P. Dommersnes, O. Orwar, and B. Akerman, Langmuir **23**, 7652 (2007).
[37] F. Campelo and A. Hernandez-Machado, Phys. Rev. Lett. **100**, 158103 (2008).
[38] J. Hurtig and O. Orwar, Soft Matter **4**, 1515 (2008).
[39] M. Deserno and W. M. Gelbart, J. Phys. Chem. B **106**, 5543 (2002).
[40] S. Tzlil, M. Deserno, W. M. Gelbart, and A. Ben-Shaul, Biophys. J. **86**, 2037 (2004).
[41] J. Benoit and A. Saxena, Phys. Rev. E **76**, 041912 (2007).
[42] W. T. Gozdz, Langmuir **23**, 5665 (2007).
[43] W. Helfrich and R.-M. Servuss, Nuovo Cimento D **3**, 137 (1984).
[44] W. Helfrich, Z. Naturforsch. C **28**, 693 (1973).
[45] U. Seifert, K. Berndl, and R. Lipowsky, Phys. Rev. A **44**, 1182 (1991).